ACS Photonics

Article

pubs.acs.org/journal/apchd5

Colloidal Quantum Dot Integrated Light Sources for Plasmon Mediated Photonic Waveguide Excitation

Jean-Claude Weeber,*[,†] Kamal Hammani,[†] Gerard Colas-des-Francs,[†] Alexandre Bouhelier,[†] Juan Arocas,[†] Arunandan Kumar,[†] Fabien Eloi,[‡] Stéphanie Buil,[‡] Xavier Quélin,[‡] Jean-Pierre Hermier,[‡] Michel Nasilowski,[§] and Benoit Dubertret[§]

[†]Laboratoire Interdisciplinaire Carnot de Bourgogne, UMR 6303 CNRS-Université de Bourgogne-Franche Comté, 9 Avenue A. Savary, F-21078 Dijon, France

[‡]Groupe d'Étude de la Matière Condensée, Université de Versailles-Saint-Quentin-en-Yvelines, Centre National de la Recherche Scientifique, UMR8635, 45 Avenue des États Unis, 78035, Versailles, France

[§]Laboratoire de Physique et d'Étude des Matériaux, Centre National de la Recherche Scientifique, UMR8213, École Supérieure de Physique et de Chimie de la ville de Paris, 10 Rue Vauquelin, 75231, Paris, France

ABSTRACT: We operate micron-sized CdSe/CdS core–shell quantum dot (QD) clusters deposited onto gold patches as integrated light sources for the excitation of photonic waveguides. The surface plasmon mode launched by the QD fluorescence at the top interface of the gold patches are efficiently coupled to photonic modes sustained by titanium dioxide ridge waveguides. We show that, despite a large effective index difference, the plasmonic and the photonic modes can couple with a very high efficiency provided the vertical offset between the two kinds of waveguides is carefully controlled. Based on the effective index contrast of the plasmonic and the photonic modes, we engineer in-plane integrated hybrid lenses. The hybrid lenses are obtained by shaping the contact interface between the plasmonic and the photonic waveguides. We demonstrate a 2-fold enhancement of the coupling efficiency for tapers equipped with a hybrid lens. Our results are expected to be useful for the development of low-cost, integrated light sources deployed in photonic circuits.

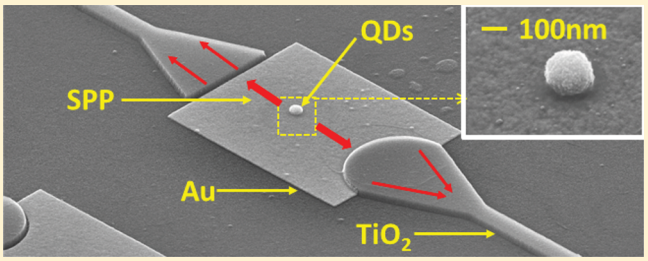

KEYWORDS: *colloidal quantum dots, surface plasmon, integrated light sources, photonic waveguides, hybrid lens, lens-assisted taper*

Fully integrated photonic devices are typically comprised of passive photonic components and active elements, including sources and detectors. The integration of solid-state light sources in photonic integrated circuits is most often an expensive and technologically challenging procedure whatever the waveguiding material platform.[1] On the other hand, colloidal quantum dots (QDs) have been identified as a cost-effective and efficient solution for the development of light emitting diodes.[2,3] Hence, whenever an incoherent, low bandwidth, broad spectrum light source is needed, colloidal QDs offer a strategic alternative to complex heterostructures. It was suggested recently that colloidal QDs could be operated as surface plasmon sources when arranged in a controlled way at the micron scale[4] or the nanoscale.[5] The interaction of colloidal QDs with waveguide modes is also reported in the literature,[6−8] but so far only little is done in the direction of hybrid plasmo-photonic coupling configurations of colloidal integrated light sources. In this work, we investigate configurations comprised of gold thin film patches optically connected to titanium dioxide (TiO_2) ridge waveguides. The QD clusters are deposited onto the metal patches and the surface plasmon modes launched by the QD fluorescence are coupled to the photonic modes of the TiO_2 waveguides. The interest of an hybrid approach for the QD fluorescence excitation of the photonic waveguides is 2-fold. First, a plasmon-assisted excitation is efficient at selecting a well controlled polarization state impinging the entrance of the photonic waveguide. Second, a hybrid configuration offers the opportunity to develop in-plane integrated micro-optics for improved light injection. Indeed, by taking advantage of the high effective index contrast between the plasmonic and the photonic modes, we show that in-plane integrated optical elements such as lenses can be implemented by a careful design of the transition surface between the metal patches and the photonic waveguides. Such configurations are of practical interest down to the single-QD level for the development of plasmon assisted integrated colloidal single-photon sources.[9] Although the hybrid plasmo-photonic configurations demonstrated in this work rely on TiO_2 waveguides, our approach is not restricted to visible spectral domain and may be extended to other waveguiding platform such as silicon-on-insulator and emitting materials (PbS QDs, for example).

Received: January 28, 2016
Published: April 4, 2016

DOI: 10.1021/acsphotonics.6b00054
ACS Photonics 2016, 3, 844−852

The study is organized as follows. We first briefly describe the fabrication of our hybrid plasmo-photonic configurations along with the procedure for the deterministic deposition of the colloidal QD clusters onto the metal films. The excitation of surface plasmon (SP) modes by means of QD fluorescence is investigated first with the help of an inverted optical microscope. Next, we show that the coupling efficiency of an SP mode incident onto a photonic waveguide mode can be close to 95% provided the vertical and lateral alignments of the two waveguides are carefully controlled. The high effective index contrast between the SP and the photonic modes sustained by our hybrid configuration is a key ingredient for the development of in-plane integrated optical elements. For instance, we show that by shaping the surface between the metal patches and the photonic waveguides, one can design in-plane integrated hybrid lenses for improved collection of the SP-coupled QD cluster fluorescence. Finally, by implementing such a hybrid lens at the input of a photonic waveguide, we demonstrate a 2-fold enhanced coupling efficiency as compared to standard taper input waveguides.

IN-PLANE INTEGRATED HYBRID PLASMO-PHOTONIC COUPLERS

A typical hybrid plasmo-photonic (HPP) configuration for coupling colloidal QD fluorescence into a photonic waveguide is shown in Figure 1a. The HPP structure is comprised of gold patches connected to titanium dioxide waveguides lying onto a glass substrate. The samples were fabricated by a two step electron-beam lithography followed by dry etching, thermal deposition and metal film lift-off processes. A typical QD cluster acting in the following as a local fluorescent source is also visible in Figure 1a. The QDs used in this work are homemade core−shell CdSe/CdS nanocrystals emitting at 670 nm (see Figure 1d) and featuring a core radius around 3 nm and a shell thickness around 10 nm. The nanocrystals dispersed in hexan were synthesized following the first step of the procedure described in Supporting Information of ref 10. The deterministic positioning of the QDs was performed following a similar approach as described in ref 11. To that aim, a third electron beam lithography step applied to a 250 nm thick poly(methyl methacrylate) (PMMA) layer was used to open micron-sized cavities at the locations where the QD clusters need be deposited. Next, the QD solution was spin-coated onto the processed PMMA layer (1500 rpm for 60 s), and finally, the unexposed PMMA layer areas were dissolved in acetone for 15 min leaving the QDs clusters at the location of the cavities. The controlled deposition process had a success rate around 75% (QD clusters are found over 75% of the expected sites). Note, however, that atomic force microscopy and scanning electron microscopy images reveal that the volume of the QD clusters is fluctuating from one deposition site to the other. The samples were optically characterized using an inverted microscope equipped with an immersion oil objective (60×, 1.49 NA) and a visible CCD camera. The QDs were excited by a continuous wave 405 nm laser diode focused onto the sample using a long working distance objective (100×, 0.52 NA). The laser diode transmitted light was filtered out using a long-pass filter with a cut-on wavelength of 650 nm. A typical image recorded with the CCD camera is shown in Figure 1c. The fluorescent source along with the scattered light spots at the output of the photonic waveguides are clearly visible demonstrating that the QD cluster deposited onto a gold patch acts as a mesoscopic light source for the excitation of photonic waveguides. The QDs being deposited on a film sustaining SP modes, their excitation by the fluorescent local source is investigated first.

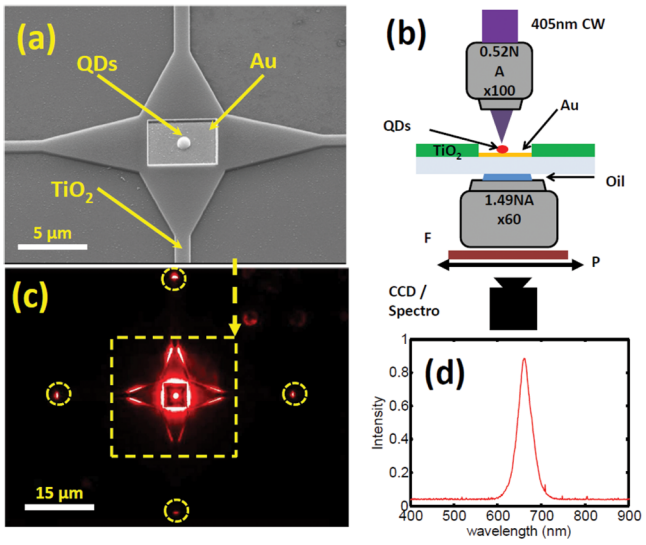

Figure 1. (a) Scanning electron microscope image of a typical hybrid plasmo-photonic configuration considered throughout the study. The samples are comprised of gold pads (thickness 65 nm) on which clusters of core−shell CdSe/CdS QDs are deposited in a controlled way. The metal film is in intimate contact with TiO_2 photonic waveguides. (b) Experimental setup operated to characterize the hybrid waveguides. The fluorescent images are formed by an immersion objective. The pump wavelength is filtered out using the long-pass filter F (cut-on 650 nm). (c) Fluorescent image obtained with the 405 nm beam focused onto the QD cluster. The coupling into the photonic waveguides is exemplified by the scattering spots (circles) at the output of each waveguides. (d) Emission spectrum of QDs pumped at 405 nm when deposited onto a glass slide.

SURFACE PLASMON MODE EXCITATION BY COLLOIDAL QD CLUSTERS

The excitation of thin-film surface plasmon by the emission of colloidal QDs was analyzed first in ref 12. More recently, the excitation of long-range SP modes by lithographically positioned QDs was demonstrated.[4] Similarly, the excitation of SP modes by means of QDs accurately positioned down to the submicron scale into trenches opened in a metal thin film was also reported in ref 5. As a key element of the plasmon−photonic hybrid configuration, we shall first investigate the properties of SP modes of metal patches when they are excited by the fluorescent emission of colloidal QD clusters.

Figures 2a and b show, respectively, a scanning electron microscope image and the corresponding fluorescent image of omni-directional plasmon metal strip waveguides with a width of 1.5 μm (thickness = 65 nm). The QD cluster is located at the center of the star-like SP waveguides arrangement. The optical pumping of the QDs at 405 nm leads to an isotropic excitation of the SP waveguides. The intensity of the scattering spot at the edge of the central circular pad (radius = 2.5 μm) is found to be 2.4× larger than the scattering spot at the output of the 10 μm-long waveguides. This is in fair agreement with the expected ratio of 2.2 inferred from the calculated $\frac{1}{e}$ damping distance of 13 μm of a gold/air thin film SP mode at a free-space wavelength of 670 nm. When placed at the center of a 17 × 17 μm^2 gold patch (see Figure 2c), the excitation of the QD

DOI: 10.1021/acsphotonics.6b00054
ACS Photonics 2016, 3, 844−852

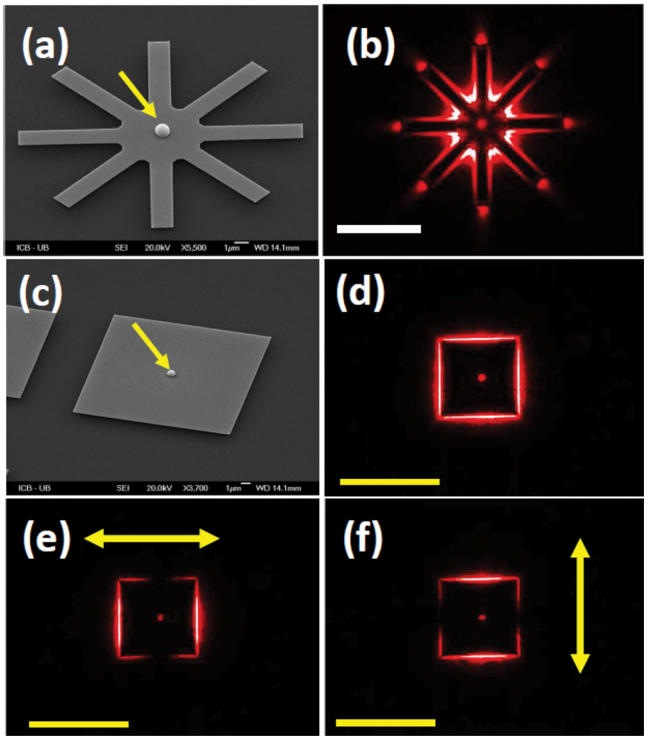

Figure 2. (a) Scanning electron microscope image of star-shaped metal stripes equipped with a QD cluster local source. (b) Fluorescent image of the star-shaped plasmonic waveguides when the QD cluster is pumped at 405 nm (scale bar = 10 μm). (c) Scanning electron image of a square gold patch equipped with a QD cluster. (d) Fluorescent image without polarization analysis of the square gold patch sustaining surface plasmon mode excited by the QD cluster (scale bar = 20 μm). (e) and (f) are the same as (d), with the polarization analyzed along the double arrow.

cluster leads to fluorescent images sensitive to polarization analysis. Indeed, as shown by Figure 2e,f, the scattering spots at the edges are dominantly observed along the axis of the analyzer, as expected for an in-plane propagating TM-polarized mode. Those observations indicate that the QD clusters deposited on top of a gold patch can be used as omnidirectional surface plasmon sources. Beyond the confirmation of surface plasmon coupled QD emission, the question of the coupling efficiency is obviously of key importance in view of practical applications. The emission properties of closely packed emitters cannot be readily obtained since it may depend on the exact shape of the cluster, the mutual interaction between the emitters within the cluster, and the nature of the coupling regime (weak or strong)[13] of the emitters with the electromagnetic modes available at the location of the cluster. The quantitative evaluation of the coupling efficiency of a QD cluster with SP modes is out of the scope of the present study. Nevertheless, as a very coarse evaluation of this coupling efficiency, we refer to the decay rate of a single dipole radiator with a fixed dipole moment facing an infinitely extended thin gold film sustaining surface plasmon modes. By using the formalism described in ref 14, one can evaluate the Au/air SP mode decay rate $\Gamma_{SP}^{\parallel,\perp}(z)$ normalized by the total decay rate $\Gamma_{tot}(z)$ for a dipole radiator placed at a distance z from the Au/air interface and for a dipole moment orientation either parallel or perpendicular to the gold film. By taking into account an averaging of the dipole moment orientation for a large number of QDs within the cluster, the normalized decay rate is given as a function of z by $\bar{\Gamma}_{SP}(z) = \frac{1}{3\Gamma_{tot}(z)}[\Gamma_{SP}^{\perp}(z) + 2 \times \Gamma_{SP}^{\parallel}(z)]$, where the factor two for $\Gamma_{SP}^{\parallel}(z)$ arises from the two possible and mutually perpendicular in-plane orientations of the dipole moment with respect to the plane of the metal film. Assuming a semispherical cluster with a radius of R deposited onto the metal film, the volume averaged SP decay rate for independent dipoles distributed homogeneously within the hemisphere can be obtained as $\Gamma_{SP}^{av} = \frac{3}{2R}\int_0^R \bar{\Gamma}_{SP}(z)\left(1 - \frac{z^2}{R^2}\right)dz$. Finally, normalizing the average SP decay Γ_{SP}^{av} to the quantum yield η of the emitter in vacuum leads to an estimate of the ratio of the power coupled into the SP mode to the power radiated by the cluster in vacuum. For a typical cluster with a radius R = 500 nm deposited onto a gold film and a quantum yield for the CdSe/CdS QDs around η = 40% at room temperature,[15] we find that up to 37% of the power radiated by cluster in vacuum is coupled into the Au/air SP mode at a free-space wavelength of 670 nm.

SURFACE PLASMON MEDIATED PHOTONIC MODES EXCITATION

The development of an hybrid plasmo-photonic coupler for QD cluster sources imposes to consider the coupling efficiency of the SP mode to the photonic mode of interest. Many configurations of SP excitation by photonic modes or vice versa were investigated so-far and are reported in the literature. For example, based on dispersion relation considerations, the coupling conditions of slab waveguide and SP thin film modes were investigated in ref 16, disregarding, however, the modal coupling efficiency. The configuration we consider is shown in Figure 3a and consists of substrate featuring topographic step with a height d_o. On one side of the step, a

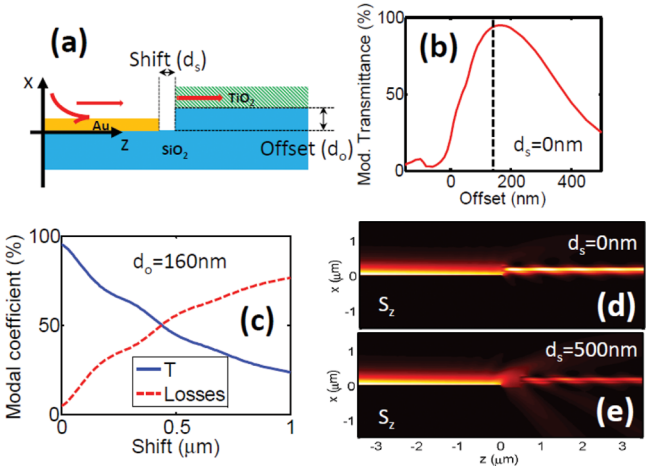

Figure 3. (a) Schematic view of the numerical situation used to investigate the coupling between a thin film SP mode and a TM-polarized photonic mode TM_0 (effective index = 1.83) sustained by a TiO_2 slab layer with a thickness of 155 nm. (b) Numerically computed modal transmission of the thin film SP mode to the photonic mode for a zero longitudinal shift d_s (see (a)). (c) Numerically computed modal transmission and losses from the SP mode to the TM_0 mode as a function of the longitudinal shift d_s when the plasmonic film is in a recessed position with respect to the photonic waveguide d_o = 160 nm. (d; respectively, (e)) Z-component Poynting vector distributions for d_o = 160 nm and d_s = 0.0 nm (respectively, d_s = 500 nm). The incident SP mode is traveling from the left to the right and couples to the TM_0 mode.

DOI: 10.1021/acsphotonics.6b00054
ACS Photonics 2016, 3, 844−852

metal film with a thickness h_m is deposited. The boundary of the metal film is longitudinally shifted by d_s with respect to the vertical flank of the step. A slab TiO_2 waveguide with a thickness h_w is lying on the upper side of the step. A SP mode traveling from the left to the right at the metal/air interface of the semi-infinite metal film is expected to butt-couple to the photonic modes with an efficiency that depends on the offset d_o and the shift d_s. Although two-dimensional, this guiding configuration is still relevant for our experimental configuration where the metal patches are wide compared to QD emission wavelength and where the photonic waveguides are tapered. We operate a homemade numerical code based on a integrated optics version of the Fourier Modal Method (FMM)[17,18] to compute the modal transmission and losses as a function of parameters d_s and d_o. The incident Au/air SP mode traveling onto the upper interface of the metal film (thickness of 65 nm) at 670 nm has a calculated effective index of $n_{eff}^{SP} = 1.037$. When the metal film is in contact with the step ($d_s = 0$ nm), the modal transmission of the SP mode to the TM_0 mode (effective index $n_{eff}^{TM_0} = 1.83$) of a 155 nm thick TiO_2 slab waveguide is below 4% when $d_o = -155$ nm corresponding to the metal film deposited on top of the TiO_2 waveguide. The coupling efficiency can be as large as 94% provided the vertical offset d_o is around 160 nm (see Figure 3b). Interestingly, for such a vertical offset, the modal coupling efficiency is found to be robust against the longitudinal shift and remains as high as 75% for $d_s = 150$ nm, making this configuration rather tolerant to fabrication deviations. The almost full transmission of the SP mode to the TM_0 photonic mode is exemplified by the Poynting vector distribution displayed in Figure 3d. When the longitudinal shift is increased to $d_s = 500$ nm, the coupling efficiency drops below 50% but the photonic waveguide excitation is still clearly visible (Figure 3e). The critical role of the vertical offset in our situation is consistent with the results reported in the case of a Silicon-On-Insulator (SOI) waveguide coupled to a dielectric-loaded surface plasmon (DLSPP) waveguide.[19] In our case, the coupling efficiency of the thin-film plasmon mode to the slab TM_0 photonic mode might sound rather large when considering the difference of effective indices for the two modes and referring to a crude approximation based on simple Fresnel formula. However, we note that a coupling efficiency as high as 80% is reported in ref 19 for the excitation of the DLSPP waveguide by a SOI waveguide in spite of a difference in effective index around 2. From our numerical results, we conclude that the gold film patch must be in a vertically recessed configuration in order to achieve a significant coupling between the SP mode and the photonic mode. We verified this conclusion experimentally by fabricating TiO_2 circular disks (radius = 15 μm) from a 152 nm thick TiO_2 layer. As shown schematically in Figure 4a,b, the TiO_2 disks are equipped with circular gold patches (radius = 2.5 μm) deposited either onto the TiO_2 layer or recessed into the TiO_2 layer. When the gold patch is deposited onto the dielectric disk (see Figure 4c), the SP mode excited at the top interface of the metal film is simply scattered at the edges of the metal film and does not couple significantly to the photonic modes. On the contrary if recessed within the dielectric disk (Figure 4d), a neat light diffusion at the rim of the dielectric disk indicates a good coupling between the SP and the photonic modes. A polarization analysis (Figure 4e,f) of the fluorescence images for the recessed configuration shows that the guided mode excited within the dielectric disc is highly TM-polarized, as expected from the coupling with an incident SP

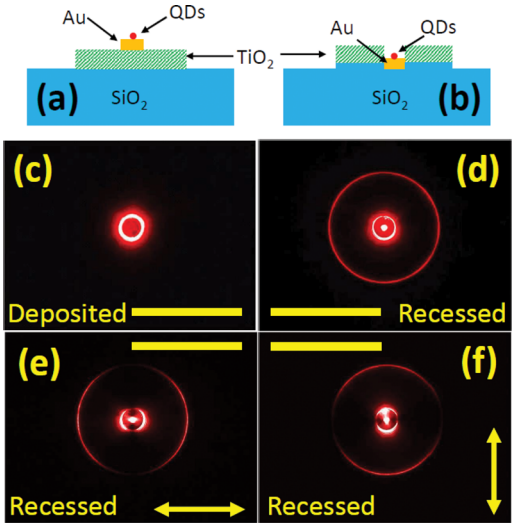

Figure 4. (a; respectively, (b)) Schematic view of a hybrid photonic disc with a plasmonic patch deposited onto (respectively, recessed into) the photonic waveguide. A QD cluster is deposited onto the plasmonic patch in both situations. (c; respectively, (d)) Fluorescent image recorded without polarization analysis when the QD cluster is pumped at 405 nm for the situation shown in (a; respectively, (b)). (e, f) Fluorescent image recorded for the recessed configuration (see (b)) with an analyzer oriented along the double arrow (scale bar = 30 μm).

mode. Note that for the dielectric disk, the fundamental mode is TE-polarized (effective index $n_{eff} = 2.08$). This result demonstrates that plasmon mediated excitation of photonic waveguides is an efficient way to select a well-defined polarization from the fluorescent emission, a situation that cannot be readily achieved if the QDs are simply directly deposited onto the photonic waveguides. Indeed in this situation both TE-polarized and TM-polarized photonic modes are excited. However, preliminary results indicate that for QDs deposited directly onto the TiO_2 disc, the excitation of the TM-polarized mode is slightly favored owing to the modal field distribution for each polarization. Nevertheless, unlike the hybrid coupling configurations, no significant polarization selection is observed for the QDs directly deposited onto the photonic waveguide.

HYBRID INTEGRATED OPTICAL COMPONENTS

Hybrid Plasmo-Photonic Lens. Polarization selection is one of the interest of a plasmon mediated excitation of photonic waveguides by local fluorescent sources. We shall show now that hybrid configurations are also useful for the implementation of in-plane integrated optical elements aimed at improving the coupling efficiency. Pure plasmonic surface optical elements were demonstrated for surface plasmon modes by adding a thin dielectric layer on top of a metal film[20] or a subwavelength structured dielectric effective medium.[21] In any case, the surface optical elements rely on a difference of effective index of the SP mode traveling at the metal/air or metal/dielectric interface. In principle, this approach can be extended to the situation of the transition from a surface plasmon mode to a photonic mode provided that the two types of mode have significantly different effective indices. In our situation, the surface plasmon mode has an effective index around 1.037, whereas the TM_0 mode for the TiO_2 waveguides can be as high as 1.8. Such a large effective index difference is, thus, favorable to the development of in-plane integrated

DOI: 10.1021/acsphotonics.6b00054
ACS Photonics 2016, 3, 844−852

optical lens featuring typical micron-sized radius of curvature and focal lengths. Figure 5a shows a schematic view of the

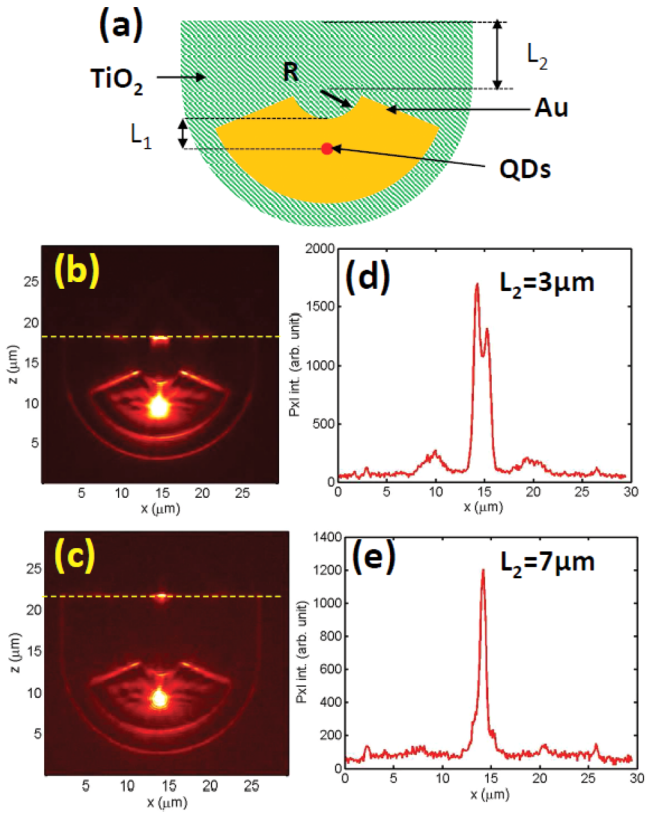

Figure 5. (a) Schematic view of the hybrid lens. The gold film is in a recessed configuration. The contact surface between the plasmonic patch and the TiO_2 layer features a circular shape with a radius R. (b; respectively, (c)) Fluorescent image obtained for a source-lens distance L_1 = 3 μm, a lens radius of R = 2.5 μm, and a distance L_2 = 3 μm (respectively, L_2 = 7 μm). (c; respectively, (d)) Intensity cross-cuts taken over the edge of the TiO_2 mesa at a distance L_2 = 3 μm (respectively, L_2 = 7 μm).

hybrid configuration fabricated to demonstrate an in-plane integrated hybrid lens. A QD cluster is deposited onto a gold thin film recessed in a TiO_2 cavity. A semicircular surface of radius R faces the QD cluster. The surface acts as a convex lens focusing the surface plasmon launched by the emission of the QDs. The distance between the local source and the summit of this lens is denoted L_1. The TiO_2 layer extends over a distance L_2 after the center of the lens. The fluorescence images displayed in Figure 5b,c were recorded for R = 2.5 μm, L_1 = 3 μm, and two different distances L_2. The intensity cross-cuts plotted, respectively, in Figure 5d,e were taken over the scattering spot at the rim of the TiO_2 mesa for L_2 = 3 μm and L_2 = 7 μm. It is clear from those two cross-cuts that the hybrid lens achieves the focusing of the fluorescence-SP coupled source. We modeled the experimental configuration by the two-dimensional situation depicted in Figure 6a. The electric intensity distribution displayed in Figure 6b was obtained by using the FMM for an incoherent illumination of a 400 nm wide slit opened in an optically opaque screen playing the role of the local experimental source. The width of the slit-source was chosen to provide a sufficient angular spreading of the emitted light to fill the numerical aperture of the microlens with a radius of 2.5 μm considered for this calculation. In addition,

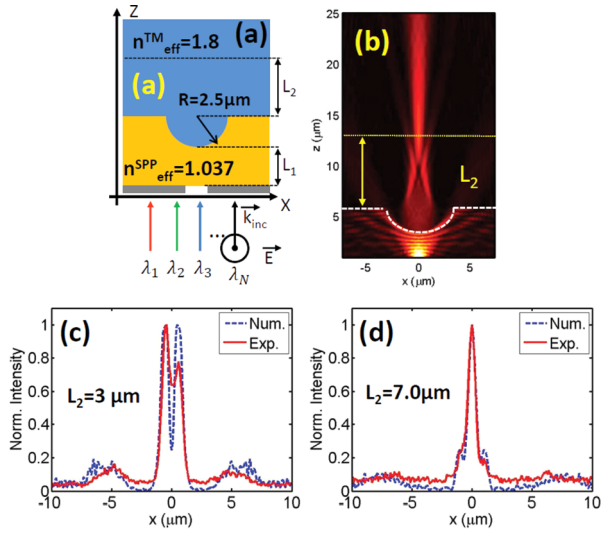

Figure 6. (a) Computation situation for the modeling of the hybrid plasmo-photonic lens. The model is two-dimensional (invariant along the Y-axis). The refractive index of each material in the model corresponds to the effective indices of the SP and the photonic modes, respectively. (b) Electric intensity distribution for an incoherent illumination of the slit mimicking the local fluorescent source in the presence of a lens of radius R = 2.5 μm. (c; respectively, (d)) Comparison of the numerical (dashed line) and experimental (solid line) intensity cross-cut for an observation distance from the lens L_2 = 3 μm (respectively, L_2 = 7 μm).

the nonvanishing lateral size of the slit light source accounts for the spatial extension of the experimental QD clusters, a property that cannot be captured by a single two-dimensional dipole line source for example. Up to 20 plane waves with free-space wavelengths ranging from 660 to 680 nm were used to simulate the broad emission spectrum of the QDs. The hybrid lens has been simulated by considering nondispersive medium with refractive index respectively equal to the SP and TM_0 mode effective index. The approximation of nondispersive SPP and photonic modes is used in this situation because of the tiny change of effective index for the two modes over the 20 nm-wide emission spectrum of the QDs. For the calculation, the TE polarization was considered given that in the experimental situation the TM-polarization corresponds to a dominant electric field component parallel to the vertical flanks of the structures. Note that the same approximation is used in the effective index method.[22] On the basis of the electric intensity field distribution displayed in Figure 6b, one can see that the microlens focuses the diverging incident beam emitted by the slit located at a distance L_1 = 3 μm from the lens. The cross-cuts of the intensity distribution taken at distances L_2 = 3 μm and L_2 = 7 μm are plotted in Figure 6c and d, respectively. The numerical cross-cuts are in good agreement with the experimental profiles recorded for the same parameters as in the numerical situation. The same good agreement was also observed for hybrid lenses with radii of 2.0 and 3.0 μm, indicating that our 2D model using the effective index of, respectively, the SP and the photonic mode is a reliable approach for modeling experimental hybrid plasmo-photonic devices.

Hybrid Lens Assisted Taper for Enhanced Waveguide Coupling. We used the 2D model to design an hybrid configuration optimized for the injection of the surface-plasmon coupled fluorescence emission into a photonic

DOI: 10.1021/acsphotonics.6b00054
ACS Photonics 2016, 3, 844−852

waveguide. The configuration we propose is a lensed hybrid taper (see Figure 7a) featuring a semicircular interface between

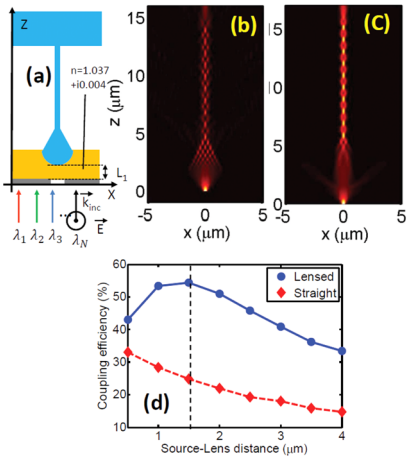

Figure 7. (a) Numerical situation for modeling local source light injection into a photonic ridge waveguide (width = 500 nm) by means of a lensed-taper. The lens has a radius of 1.5 μm and the taper region is 3.0 μm wide and 3.0 μm long. The homogeneous medium on top of the waveguide is used to minimize the back-reflection of the guided mode at the termination of the waveguide. (b; respectively, (c)) Poynting vector Z-component distributions computed for an incoherent illumination of a straight taper (respectively lensed-taper) for a source-lens distance L_1 = 1.5 μm. (d) Coupling efficiency (relative to the power emitted by the local source) into the waveguide as a function of the source-lens distance for the lensed-taper (solid line) and straight taper (dashed-line) terminated waveguide.

the metal film and the photonic waveguide in addition to the standard taper for transition from the slab to the ridge waveguide mode. Such a lens-assisted taper configuration was originally proposed in the context of silicon-on-insulator optics for focusing the fundamental mode of a wide ridge waveguide. Although the numerical aperture of the integrated lens was set to match the numerical aperture of the waveguide, the benefit of such a lensed configuration compared to a standard straight entrance interface taper configuration was rather moderate.[23] However, we show in the following that a lensed taper implemented in the hybrid configuration discussed here provides a significant improvement of the coupling efficiency. Figure 7b,c show the amplitude of the z-component S_z of the Poynting vector for a distance L_1 = 1.5 μm between the local source and a 500 nm wide waveguide. In Figure 7b, the input of the waveguide is a standard straight entrance interface taper (denoted hereafter as straight taper), while in Figure 7c, the taper has a semicircular front surface. For the width considered here, the waveguide sustains two TE-polarized modes leading to the characteristic dual-mode beating distributions observed in Figure 7b,c. From these two images, displayed with the same color scale, it is clear that the lensed-taper provides a better coupling into the waveguide than the straight taper configuration. This improvement results from the focusing of the strongly diverging beam formed by the local source. The lensing effect is even more clearly demonstrated in Figure 7d showing the ratio of the power coupled into the waveguide to the power emitted by the local source in the case of the lensed-taper waveguide (solid line) and straight taper waveguide (dashed line). For the straight taper, the coupled power decreases continuously with the source-waveguide distance whereas an optimum coupling distance is obtained with the lensed-taper at L_1 = 1.5 μm. Note that a numerical approach is necessary for the design of the hybrid lens since basic geometrical optic considerations lead to a highly overestimated optimum distance (L_1 = 12 μm) owing to the combined effects of the spatial extension and high angular divergence of the local light source. The sample shown in Figure 8a was fabricated

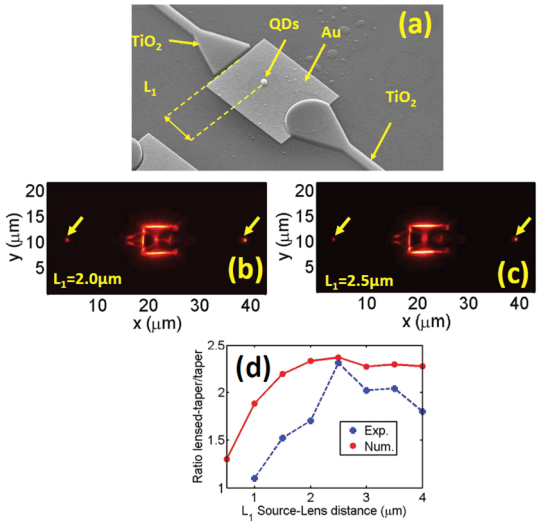

Figure 8. (a) Scanning electron image of the sample used to demonstrate the enhanced waveguide lightwave injection using a lensed-taper coupling region. (b; respectively, (c)) Fluorescent image showing the scattering spots at the output of the two TiO_2 ridge waveguides equipped respectively with a straight (left) and lensed (right) tapers for a source distance L_1 = 2.0 μm (respectively, L_1 = 2.5 μm). (d) Dashed line: Ratio of the average scattering spot intensity at the output of each waveguide as a function of the source distance L_1. Solid line: Ratio of numerically evaluated coupled power for in the case of a waveguide equipped with a lensed-taper and a straight taper (see text).

using the opto-geometrical parameters extracted from the numerical results of our 2D model. A QD cluster is deposited onto a gold thin film connected to two TiO_2 waveguides of same length facing each other and equipped respectively with a standard taper or a lensed-taper coupling region. The source is placed at the same distance L_1 from the edge of straight taper and the summit of the cylindrical lens. The fluorescent images recorded for a distance L_1 = 2.0 μm and L_1 = 2.5 μm are displayed in Figure 8b and c, respectively. From the scattering spots visible at the output of each waveguide, it is clear that light injection of the local source is more efficient with the lensed-taper. In fact, the role of the lens implemented at the entrance of the taper can be directly observed on the experimental images of Figure 8b,c. Light propagation in the standard taper leads to multiple scattering with the edges. The contour of the coupling region is readily visible and indicates the presence of losses. For the lensed-taper, the edges of the taper are no longer visible. This observation is consistent with the numerically computed Poynting vector distributions displayed in Figure 7b,c. As noted before, the focusing of the local light source by the integrated lens mitigates light leakage at the tilted edges of the (nonoptimized) taper. Unlike the numerical situation, the power coupled into the waveguides for each distance L_1 in the experimental situation cannot be directly compared given that the QD clusters deposited on each device are not strictly similar. However, by taking the ratio of

DOI: 10.1021/acsphotonics.6b00054
ACS Photonics 2016, 3, 844−852

the scattered intensity at the output of the two waveguides for each distance L_1, the dashed-line curve plotted in Figure 8d is obtained. From this curve, we conclude that light injection into the photonic waveguide is more than twice efficient with the lensed-taper than for the straight taper for a distance L_1 equal to 2.5 μm. The numerical evaluation of the ratio of the power coupled into a waveguide equipped with a straight or a lensed taper was performed on the basis of the results displayed in Figure 7d. The numerical model leads to an overestimate of the power ratio for all source-waveguide distances but captures however the experimental trend with an optimum ratio at L_1 = 2.5 μm, in agreement with the experimental data. The main origin for this discrepancy may be the definition of the source-waveguide distance. For the experimental QD clusters the source-waveguide distance is averaged over the size of the cluster, a situation that is not taken into account by the slit-source model. Nevertheless, the qualitative agreement between experimental and the numerical results suggests that our 2D model approach is useful at parametrizing the initial design of plasmo-photonic device.

CONCLUSION

In summary, we introduce a hybrid plasmo-photonic platform for efficiently capturing the local fluorescent signal emitted by a cluster of colloidal QDs. The samples were obtained by a multistep electron-beam lithography process for the fabrication of the photonic waveguides, plasmonic patches and the deterministic deposition of the QD clusters onto the plasmonic patches. We showed that a QD cluster can be operated as an efficient, local, isotropic SP sources. Once coupled to the SP modes, the excitation of the photonic mode by the QD cluster can be highly efficient provided the plasmonic patch is in a recessed configuration compared to the photonic waveguide. The optimum vertical offset for the excitation of the photonic mode by an incident SP mode is in the range of 160 nm for TiO_2 waveguides considered in this work. Interestingly, we note that the coupling efficiency between the incident SP mode and the photonic mode is rather robust against a longitudinal shift of the two waveguides making such hybrid configurations fabrication tolerant. Next, we showed that the mediation of the plasmon mode enables a polarization selection of the photonic modes. While the fundamental mode of the photonic waveguide is TE polarized, the excitation via the surface plasmon preferentially selects the TM modes of the waveguide. This is of advantage for controlling the polarization state of an otherwise unpolarized fluorescent source.

Furthermore, one can take advantage of the large effective index contrast between the SP and photonic modes to implement in-plane integrated optical components aimed at improving the collection efficiency of the photonic waveguides. In particular, we demonstrated lensing effect of a circularly shaped transition from the plasmonic patch to the photonic waveguide. Finally, we proposed a lensed-taper design showing superior performances for light injection from the QD cluster into the photonic waveguides than standard taper. The results we report in this work are expected to be valuable for the development of low-cost integrated light sources in the context of practical applications ranging from integrated colloidal single-photon sources to alignment-free massively parallel integrated optical biosensors.

METHODS

Sample Fabrication. The fabrication of the samples started by the deposition of a 155 nm TiO_2 layer onto a 170 μm thick microscope glass cover plate. The deposition was performed by reactive radio frequency magnetron sputtering applied onto a 99.9% pure titanium target and using a mixture of pure argon and pure oxygen. The procedure used for the deposition is expected to provide amorphous TiO_2,[24] however subsequent Raman spectroscopy measurements indicate that we obtained mostly anatase crystalline TiO_2. After TiO_2 layer deposition, a first electron beam lithography process is conducted onto a 250 nm thick PMMA layer (molecular weight 950 K) spin-coated onto the TiO_2 layer at 3500 rpm for 60 s and baked out at 170 °C for 3 min. After deposition of a thin gold conducting layer on top of the PMMA layer, the electron-beam lithography was performed at an acceleration voltage of 20 kV whereas the dose was computed for an emission current of 35pA and using an apparent resist sensitivity of 250 $\mu C/cm^2$. After development of the exposed resist, the substrate was coated by electron-gun evaporation with a 30 nm thick nickel layer which was subsequently lifted-off. The remaining Ni patterns were used as etching masks during the dry etching of the TiO_2 layer performed by reactive ion etching using a mixture of pure argon and sulfur hexafluorid gas. During this process, the etching rate of the TiO_2 layer was 50 nm per minute. The etching process was stopped after an overetching depth of the glass substrate of about 170 nm. For the fabrication of the hybrid structures, the deposition of the gold patterns was done by a second overlay lithography process by using alignment marks surrounding the patterns of interest and thermal evaporation (pressure 10^{-7} mbar) of a 65 nm thick pure gold layer. After lift-off of the gold layer, the samples were ready for the controlled deposition of the quantum dots clusters. A third overlay electron-beam lithography process was then conducted once again on a 250 nm thick PMMA layer. Next, the samples were placed in an oxygen plasma cleaner for 1 min to remove the thin layer of exposed resist potentially remaining after the development step. A 50 μL droplet of CdSe/CdS QD dispersed in hexan was then deposited onto the processed sample and spin-coated at a speed of 1500 rpm for 60 s. Finally, the unexposed PMMA layer was dissolved in aceton for 15 min at a temperature of 60 °C. After lift-off of the resist, the QD clusters firmly attached to the gold surface. The origin of the attachment process is related to hydrophobic binding, as described in ref 11. Typical clusters are of semispherical shape with a radius around 200−300 nm leading to a rough estimate of 1000 QDs per clusters. Note that the attachment of the QD clusters onto the gold surface was so strong that megasonic cleaning attempts for recycling gold surfaces were unsuccessful.

Modeling Using the Fourier Modal Method. Home-made numerical codes were used to evaluate the coupling efficiency of a thin film surface plasmon mode to the TM_0 mode sustained by the 165 nm-thick TiO_2 layer. Those codes are based on an integrated optics version of the Fourier Modal Method applying onto periodic object.[17,18] In our case, an artificial period (along the x-direction, see Figure 3a) for the system of 15 μm was used in the computations. Given the exponential decay of both the surface plasmon mode and the photonic mode of interest at a free-space wavelength of 670 nm, such a period is large enough to prevent any significant influence of the periodicity of the system. Nevertheless, we further minimize the possible contribution of the periodicity by

DOI: 10.1021/acsphotonics.6b00054
ACS Photonics 2016, 3, 844−852

implementing 1 μm thick absorbing boundary layers[25] at the borders of the computational windows. When using the integrated optics version of the FMM, the incident field is directly an eigenmode of the entrance waveguide in such a way that there is no need for the computation to expand this eigenmode into a sum of plane waves. In our situation, the eigenmode of the entrance waveguide (comprised of a gold film deposited onto a glass substrate) is a unit amplitude SPP mode traveling at the gold/air interface. Knowing the scattering matrix of the intermediate waveguiding configuration connecting the entrance waveguide to the exit waveguide (in our case, the TiO_2 slab waveguide), the field transmitted through (respectively reflected by) the intermediate waveguiding structure (in our case a air gap of different widths d_s) can be readily computed and projected onto the eigenmodes of the output waveguide (respectively, the entrance waveguide). For example, if $t^{SPP}_{TM_0}$ denotes the amplitude of the transmitted field projected onto the TM_0 mode of the slab waveguide for a unit amplitude incident SPP mode, then the modal transmission coefficient of the SPP mode to the TM_0 mode through the intermediate waveguiding structure is given by $|t^{SPP}_{TM_0}|^2$.

For modeling the hybrid in-plane integrated optical elements such as lenses and lensed-tapers, we use this time a plane-wave version of the Fourier Modal Method relying on the S-algorithm described in ref 26. Once again the object was periodic (period = 15 μm) and up to 601 plane waves were used in the plane-wave expansion of the periodic electromagnetic fields. To simulate the incoherent nature of QD fluorescence, 20 incident plane-waves with free-space wavelengths ranging from 660 to 680 nm were used. The intensity distributions corresponding to this broad illumination spectrum were obtained by summing the intensity distributions computed for each incident plane waves. A 400 nm wide slit opened in an opaque screen was used to simulate the QD cluster local light source. We emphasize that the slit-source was used in the calculations in an uncoupled configuration. In this way, the light scattered back by the waveguides did not impact the incident light coming out from the slit. This procedure was necessary to prevent from the creation of an artificial optical Perot-Fabry cavity between the source-slit and the input interface of the straight or the lensed taper equipped waveguides.

AUTHOR INFORMATION

Corresponding Author

*E-mail: jcweeber@u-bourgogne.fr. Phone: +33 (0) 380 396 031. Fax: +33 (0) 380 396 024.

Notes

The authors declare no competing financial interest.

ACKNOWLEDGMENTS

This work is supported by the Agence Nationale de la Recherche (Grant QDOTICS ANR-12-BS-10 008), LabeX Action and Conseil Régional de Bourgogne (PARI-SMT3 program). Numerical calculations were performed using DSI-CCUB resources. Samples were fabricated using the ARCEN nanofabrication platform. J.-C.W. thanks Patrice, Evelyne, Nathalie, and Pierre-Yves for inspiring discussions.

REFERENCES

(1) Vivien, L.; Lorenzo, P. *Handbook of Silicon Photonics*; CRC Press, 2013.

(2) Shirasaki, Y.; Supran, G. J.; Bawendi, M. G.; Bulović, V. Emergence of colloidal quantum-dot light-emitting technologies. *Nat. Photonics* **2012**, *7*, 13−23.

(3) Goldberg, D.; Menon, V. M. Enhanced amplified spontaneous emission from colloidal quantum dots in all-dielectric monolithic microcavities. *Appl. Phys. Lett.* **2013**, *102*, 081119.

(4) Miyata, M.; Takahara, J. Colloidal quantum dot-based plasmon emitters with planar integration and long-range guiding. *Opt. Express* **2013**, *21*, 7882−7890.

(5) Kress, S. J. P.; Richner, P.; Jayanti, S. V.; Galliker, P.; Kim, D. K.; Poulikakos, D.; Norris, D. J. Near-field light design with colloidal quantum dots for photonics and plasmonics. *Nano Lett.* **2014**, *14*, 5827−5833.

(6) Foell, C. A.; Schelew, E.; Qiao, H.; Abel, K. A.; Hughes, S.; van Veggel Frank, C. J. M.; Young, J. F. Saturation behavior of colloidal PbSe quantum dot exciton emission coupled into silicon photonic circuits. *Opt. Express* **2012**, *20*, 10453−10459.

(7) Xie, W.; Zhu, Y.; Aubert, T.; Verstuyft, S.; Hens, Z.; Van Thourhout, D. Low-loss silicon nitride waveguide hybridly integrated with colloidal quantum dots. *Opt. Express* **2015**, *23*, 12152−12160.

(8) Omari, A.; Geiregat, P.; Dries, V. T.; Zeger, H. Light absorption in hybrid silicon-on-insulator/quantum dot waveguides. *Opt. Express* **2013**, *21*, 23272−23285.

(9) Bermùdez-Ureña, E.; Gonzalez-Ballestero, C.; Geiselmann, M.; Marty, R.; Radko, I. P.; Holmgaard, T.; Alaverdyan, Y.; Moreno, E.; J, G.-V. F.; Bozhevolnyi, S. I.; Quidant, R. Coupling individual quantum emitters to channel plasmons. *Nat. Commun.* **2015**, *6*, 7883.

(10) Ji, B.; Giovanelli, E.; Habert, B.; Spinicelli, P.; Nasilowski, M.; Xu, X.; Lequeux, N.; Hugonin, J.-P.; Marquier, F.; Greffet, J.-J.; Dubertret, B. Non-blinking quantum dot with a plasmonic nanoshell resonator. *Nat. Nanotechnol.* **2015**, *10*, 170−175.

(11) Park, Y.; Young-Geun, R.; Kim, U. J.; Chung, D.-Y.; Suh, H.; Kim, J.; Cheon, S.; Lee, J.; Kim, T.-H.; Cho, K.-S.; Lee, C.-W. Nanoscale patterning of colloidal quantum dots on transparent and metallic planar surfaces. *Nanotechnology* **2012**, *23*, 355302.

(12) Gryczynski, I.; Malicka, J.; Jiang, W.; Fischer, H.; Chan, W. C. W.; Gryczynski, Z.; Grudzinski, W.; Lakowicz, J. R. Surface plasmon coupled emission of quantum dots. *J. Phys. Chem. B* **2005**, *109*, 1088−1093.

(13) Gòmez, D. E.; Vernon, K. C.; Mulvaney, P.; Davis, T. J. Surface plasmon mediated strong exciton-photon coupling in semiconductor nanocrystals. *Nano Lett.* **2010**, *10*, 274−278.

(14) Chance, R. R.; Prock, A.; Silbey, R. Molecular fluorescence and energy transfer near interfaces. *Adv. Chem. Phys.* **1978**, *37*, 1.

(15) Javaux, C.; Mahler, B.; Dubertret, B.; Shabaev, A.; Rodina, A. V.; Efros, A. L.; Yakovlev, D. R.; Liu, F.; Bayer, M.; Camps, G.; Biadala, L.; Buil, S.; Quelin, X.; Hermier, J.-P. Thermal activation of non-radiative Auger recombination in charged colloidal nanocrystals. *Nat. Nanotechnol.* **2013**, *8*, 206−213.

(16) Ditlbacher, H.; Galler, N.; Koller, D.; Hohenau, A.; Leitner, A.; Aussenegg, F.; Krenn, J. Coupling dielectric waveguide mode to surface plasmon polaritons. *Opt. Express* **2008**, *16*, 10455−10461.

(17) Lalanne, P.; Silberstein, E. Fourier-modal methods applied to waveguide computational problems. *Opt. Lett.* **2000**, *25*, 1092−1094.

(18) Silberstein, E.; Lalanne, P.; Hugonin, J.-P.; Cao, Q. Use of grating theories in integrated optics. *J. Opt. Soc. Am. A* **2001**, *18*, 2865−2875.

(19) Briggs, R. M.; Grandidier, J.; Burgos, S. P.; Feigenbaum, E.; Atwater, H. A. Efficient coupling between dielectric-loaded plasmonic and silicon photonic waveguides. *Nano Lett.* **2010**, *10*, 4851−4857.

(20) Hohenau, A.; Krenn, J. R.; Stepanov, A. L.; Drezet, A.; Ditlbacher, H.; Steinberger, B.; Leitner, A.; Aussenegg, F. R. Dielectric optical elements for surface plasmons. *Opt. Lett.* **2005**, *30*, 893−895.

(21) Devaux, E.; Laluet, J.-Y.; Stein, B.; Cyriaque, G.; Ebbesen, T.; Weeber, J.-C.; Dereux, A. Refractive micro-optical elements for surface plasmons: from classical to gradient index optics. *Opt. Express* **2010**, *18*, 20610−20619.

DOI: 10.1021/acsphotonics.6b00054
ACS Photonics 2016, 3, 844−852

(22) Holmgaard, T.; Bozhevolnyi, S. I. Theoretical analysis of dielectric-loaded surface plasmon-polariton waveguides. *Phys. Rev. B: Condens. Matter Mater. Phys.* **2007**, *75*, 245405.
(23) Van Acoleyen, K.; Baets, R. Compact lens-assisted focusing tapers fabricated on silicon-on-insulator. 2011 IEEE/Photonics Society 8th International Conference on Group IV Photonics, England, Sept. 14−16, 2011, IEEE, 2011; pp 157−159.
(24) Bradley, J. D. B.; Evans, C. C.; Choy, J. T.; Reshef, O.; Deotare, P. B.; Parsy, F.; Phillips, K. C.; Loncar, M.; Mazur, E. Submicrometer-wide amorphous and polycristalline anatase TiO_2 waveguides for microphotonic devices. *Opt. Express* **2012**, *20*, 23821−23831.
(25) Hugonin, J.-P.; Lalanne, P.; Del Villar, I.; Matias, I. Fourier modal methods for modeling optical dielectric waveguides. *Opt. Quantum Electron.* **2005**, *37*, 107−119.
(26) Li, L. Formulation and comparison of two recursive matrix algorithms for modeling layered diffraction gratings. *J. Opt. Soc. Am. A* **1996**, *13*, 1024−1034.

DOI: 10.1021/acsphotonics.6b00054
ACS Photonics 2016, 3, 844−852